南京航空航天大学

论文集

（二〇〇九年） 第6册

能源与动力学院

（第1分册）

南京航空航天大学科技部编

二〇一〇年五月

能源与动力学院

021

目录

序号	姓名	职称	单位	论文题目	刊物、会议名称	年、卷、期
1	吴晴 钟易成 余少志 胡骏	博士生 副高 副高 正高	021 021 021 021	基于LU-SGS的非结构弹簧网格迭代算法	计算物理	2009年26卷6期
2	吴晴 钟易成 胡骏 余少志	博士生 副高 正高 副高	021 021 021 021	Navier-Stocks Computations of Wind-Turbine Airfoil using Low Mach Number Preconditioning	IEEE Asia-Pacific Power and Energy Engineering Conference 2009	2009湖北武汉
3	卞刚 钟易成 刘德刚	硕士生 副高 硕士生	021 021 021	基于CATIA/CAA的飞机燃油系统管路设计仿真	计算机辅助工程	2009年18卷3期
4	钟易成 张荣学 雷华 刘飞	副高 副高 中级 硕士生	021 021 021 021	拉瓦尔喷管实验数据采集系统建设	江苏航空	2009年1期
5	刘德刚 钟易成 卞刚	硕士生 副高 硕士生	021 021 021	等温不可压流体系统稳态数值计算方法研究	飞机设计	2009年29卷1期
6	吴晴 钟易成 胡骏 余少志	博士生 副高 正高 副高	021 021 021 021	基于激波拟合与柔性壁的反设计数值方法研究	空气动力学学报	2009年27卷2期
7	姚尚宏 雷雨冰 朱岩	硕士生 副高 本科生	021 021 021	头部旋涡蒸发管式直径6cm环形燃烧室设计和试验	航空动力学报	2009年24卷12期
8	谢庆 连亮 雷雨冰	硕士生 本科生 副高	021 021 021	基于知识工程的燃烧室初步构型设计自动化系统	中国航空学会第八届小发动机学术会议	2009江苏南京
9	尚麒麟 王德义 雷雨冰	硕士生 本科生 副高	021 021 021	波纹式微型蒸发管内的燃油射流雾化数值模拟	中国航空学会第八届小发动机学术会议	2009江苏南京
10	陈杰 黄国平 朱亮聪 张强	博士生 正高 硕士生 硕士生	021 021 021 021	Development of a New-Style Micro Diffuser	Proceedings of ASME Turbo Expo 2009	2009美国奥兰多
11	邱建 宫建光 夏晨 黄国平	硕士生 外单位 博士生 正高	021 外单位 021 021	一种微型涡轮发动机导向器改进方案	第十二届推进系统气动热力学专业学术交流会	2009年四川成都
12	刘大 黄国平 李博	硕士生 正高 副高	021 021 021	RBCC引射模态进气系统性能初步分析	第十二届推进系统气动热力学专业学术交流会	2009四川成都
13	曹传军 黄国平 王家广 邱建	博士生 正高 硕士生 硕士生	021 021 021 021	有/无叶尖间隙毫米级平面叶栅实验研究	第十二届推进系统气动热力学专业学术交流会	2009四川成都
14	徐惊雷 刘凯礼 张堃元	正高 本科生 正高	021 021 021	过膨胀超声速冲击射流中非定常现象的PIV实验与数值模拟研究	全国力学大会	2009河南郑州
15	徐惊雷 马钊 张堃元 莫建伟 李超	正高 硕士生 正高 硕士生 硕士生	021 021 021 021 021	不同过膨胀程度下非对称大膨胀比喷管的实验对比研究	第二届高超声速科技学术会议	2009安徽黄山
16	莫建伟 徐惊雷 李超 张堃元	硕士生 正高 硕士生 正高	021 021 021 021	The Design and Numerical Study of the Over-Under TBCC Exhaust System	45th AIAA/ASME/SAE/ASEE Joint Propulsion Conference & Exhibit	2009美国丹佛
17	马静 徐惊雷 郭锐 张堃元	硕士生 正高 硕士生 正高	021 021 021 021	PIV Experimental and Numerical Study of A 2-D Airfoil for Wing Turbines	2009国际风能大会暨技术和设备展览会	2009中国南京
18	李超 徐惊雷 莫建伟 张堃元	硕士生 正高 硕士生 正高	021 021 021 021	Numerical Study of the Unsteady Mode Transition Process of an Over-Under TBCC Exhaust System	45th AIAA/ASME/SAE/ASEE Joint Propulsion Conference & Exhibit	2009美国丹佛

目录

序号	姓名	职称	单位	论文题目	刊物、会议名称	年、卷、期
19	张晨凯 胡骏 刘德龙 马超	硕士生 正高 硕士生 硕士生	021 021 021 021	A Study of Wind Turbine Blades Optimization Based on Rotational Speed Control Model	第一届世界非并网风电与能源大会	2009中国南京
20	曲浩 胡骏 张晨凯	硕士生 正高 硕士生	021 021 021	The Impact of Reynolds Number on Two-Dimensional Aerodynamic Airfoil Flow	第一届世界非并网风电与能源大会	2009中国南京
21	高翔 胡骏	博士生 正高	021 021	Numerical Research of Reynolds Number Impact on Scale Model of Wind Turbine	第一届世界非并网风电与能源大会	2009中国南京
22	刘德龙 胡骏	硕士生 正高	021 021	Blade Design for Horizantal Axis Variable Speed Wind-Driven Generator	第一届世界非并网风电与能源大会	2009中国南京
23	李亮 胡骏 蒋大志 赵运生	博士生 正高 硕士生 博士生	021 021 021 021	积分时间尺度对压气机稳定性影响的数值计算研究	第十二届推进系统气动热力学专业学术交流会	2009四川成都
24	赵运生 胡骏 李亮 罗钜	博士生 正高 博士生 博士生	021 021 021 021	涡扇发动机气动稳定性的数值模拟研究	第十二届推进系统气动热力学专业学术交流会	2009四川成都
25	王志强 张环 胡骏 屠宝锋	博士生 博士生 正高 博士生	021 021 021 021	压气机二维可压缩气动稳定性分析模型	航空动力学报	2009年24卷11期
26	靳允立 胡骏	硕士生 正高	021 021	翼型失速及雷诺数变化对风力机气动性能影响的数值研究	太阳能学报	2009年30卷9期
27	张环 胡骏 刘大响 屠宝锋 王志强	博士生 正高 院士 博士生 博士生	021 021 二院 021 021	旋转总压畸变对压气机稳定性影响的二维不可压缩模型	航空动力学报	2009年24卷8期
28	屠宝锋 胡骏 赵勇	博士生 正高 博士生	021 021 021	轴流压气机动态失速过程三维计算	航空动力学报	2009年24卷7期
29	李亮 胡骏 王志强 屠宝锋	博士生 正高 博士生 博士生	021 021 021 021	多种形式插板的压气机进气总压畸变实验	航空动力学报	2009年24卷4期
30	丁建国 胡骏 蔡显新	博士生 正高 研究员	021 021 608所	某复合掠形风扇设计与内外函数值模拟研究	航空动力学报	2009年24卷3期
31	翟贤超 胡骏 王志强	硕士生 正高 博士生	021 021 021	高压压气机低速模拟试验与随动位移测量机构设计	燃气涡轮试验与研究	2009年22卷2期
32	靳允立 胡骏	硕士生 正高	021 021	叶片弯掠对多级风扇气动性能的影响	推进技术	2009年30卷1期
33	屠宝锋 胡骏 王志强 李亮	博士生 正高 博士生 博士生	021 021 021 021	低速轴流压气机旋转失速特性试验	航空动力学报	2009年24卷1期
34	章嘉麟 周正贵 邱名	硕士生 正高 硕士生	021 021 021	Design and Research of High-Performane Low-Speed Wind Turbine Blades	第一届世界非并网风电与能源大会	2009中国南京
35	邱名 周正贵 章嘉麟	硕士生 正高 硕士生	021 021 021	Three-Dimensional Flow Simulation for Horizontal Axis Wind Turbine	第一届世界非并网风电与能源大会	2009中国南京
36	周正贵 汪光文	正高 博士生	021 021	超声速风扇叶型设计研究	航空动力学报	2009年24卷1期
37	汪光文 周正贵	博士生 正高	021 021	多层设计参数的叶型气动优化	南京航空航天大学学报	2009年41卷1期
38	张航 谭慧俊	硕士生 正高	021 021	类X-47狭缝式进气道的流动特性与工作性能	航空学报	2009年30卷12期
39	周慧晨 谭慧俊	硕士生 正高	021 021	复杂变截面进气道的一种设计方法	航空动力学报	2009年24卷6期
40	谭慧俊 孙姝	正高 副高	021 071	Oscillatory Flows of Rectangular Hypersonic Inlet Unstart Caused by Downstream Mass-Flow choking	Journal of Propulsion and Power	2009年25卷1期
41	袁化成 郭荣伟	中级 正高	021 021	矩形截面高超声速进气道气动设计及实验验证	南京航空航天大学学报	2009年41卷4期

目录

序号	姓名	职称	单位	论文题目	刊物、会议名称	年、卷、期
42	袁化成 梁德旺 郭荣伟 李博	中级 正高 正高 副高	021 021 021 021	反压作用下等直隔离段性能估算	航空动力学报	2009年24卷11期
43	王卫星 袁化成 黄国平 梁德旺	博士生 中级 正高 正高	021 021 021 021	抽吸位置对高超声速进气道起动性能的影响	航空动力学报	2009年24卷3期
44	袁化成 江海 刘栋梁 郭荣伟	中级 中级 副高 正高	021 420厂 420厂 021	成发集团某系列TRT机组进排气蜗壳数值仿真研究	中航工业余压余热回收利用及高效节能装置产业发展论坛	2009四川成都

第 26 卷 第 6 期
2009 年 11 月

计 算 物 理
CHINESE JOURNAL OF COMPUTATIONAL PHYSICS

Vol.26, No.6
Nov., 2009

[文章编号] 1001-246X(2009)06-0806-07

基于 LU-SGS 的非结构弹簧网格迭代算法

吴 晴, 钟易成, 余少志, 胡 骏

(南京航空航天大学能源与动力学院, 江苏 南京 210016)

[摘 要] 针对运动间断拟合中需频繁更新网格点位置的特点, 提出一种基于 LU-SGS (lower-upper symmetric Gauss-Seidel) 迭代方法的非结构弹簧网格运动算法. 根据弹簧网格原理构建与网格拓扑关系相对应的稀疏系数矩阵, 将 LU-SGS 思想成功引入动网格迭代算法, 并辅以合理的网格运动管理策略, 实现动网格的快速迭代. 研究表明, 在非结构网格下, LU-SGS 算法可以满足运动间断拟合的需求, 在流场隐式时间推进时, 仍能保证获得稳定解; 与传统的 SOR 方法相比, 计算时耗减少 20% 以上.

[关键词] 动网格; LU-SGS; 弹簧模型; 间断拟合; 计算流体力学

[中图分类号] O241 [文献标识码] A

0 引言

网格技术包括网格生成技术[1]和网格运动技术,运动网格技术通常用于非定常流动的数值模拟,目前较为流行且应用较广泛的是基于弹簧模型的动网格算法[2,3]. 采用运动间断数值拟合方法求解定常流场时[4], 同样需要以运动网格技术为基础,并且对运动网格的计算速度和管理策略提出了新的要求.

一般认为,应用于非定常问题的运动网格技术首先关心的是运动网格质量.由于非定常问题只在物理时间步之间变化计算域,而每一物理时间步下往往需要计算几百甚至上千个伪时间步,运动网格计算耗时仅占总时耗的 1% 以下.因此,在非定常问题下,大多数基于弹簧模型的动网格技术都没有对时耗提出过多要求,相关研究也不多见.网格迭代算法一般采用 SOR 算法,其他求解方法基本未见采用.

本文采用的运动间断拟合方法在文[4]中已有详述,系以变化的计算域和运动的间断边界模拟含有间断的定常流动.在每一个时间步后均需要根据运动间断条件移动运动边界网格,并更新整个计算区域网格点坐标,故在保持网格质量的同时,迫切希望能够减少运动网格的耗时.同时,网格运动方式也较一般的非定常问题复杂,需要采用恰当的管理策略.

本文根据弹簧网格模型原理,建立了网格拓扑关系与弹簧网格模型稀疏系数矩阵的映射关系,给出了该稀疏系数矩阵构建方法,将 LU-SGS 方法引入非结构运动网格的求解过程中,有效改进了动网格算法,缩短了计算时耗,提高了运动间断数值拟合算法的工程应用价值,同时将现有的运动间断拟合技术从显式求解[4]推广到隐式时间推进算法,提出了合理的网格管理策略,进一步提高了该算法的实效性和通用性.

1 弹簧模型

弹簧模型的本质就是依据弹簧受力平衡构建合理的相邻网格点位移关系[3],即通过在网格边上虚拟一个弹簧,通过各弹簧受力平衡构建线性方程组

$$\boldsymbol{A}\boldsymbol{q} = \boldsymbol{B}, \tag{1}$$

其中 $\boldsymbol{q} = [q_1 \quad q_1 \quad \cdots \quad q_n]^{\mathrm{T}}$, 为各节点位移量(边界节点位移量为已知条件, n 为网格点个数), $\boldsymbol{B} = [B_1 \quad B_2 \quad \cdots \quad B_n]^{\mathrm{T}}$ 为非齐次项,平衡态下的弹簧网格模型 $\boldsymbol{B} = 0$. $\boldsymbol{A}$ 矩阵($n \times n$)为位移系数稀疏矩阵,其非零元素取决于网格点标号及其拓扑关系,见图 1.

[收稿日期] 2008-06-17; [修回日期] 2008-12-06

[基金项目] 总装预研基金(51413050204HK0206)资助项目

[作者简介] 吴晴(1981-),男,安徽合肥,博士生,从事进气道设计、计算流体力学方面的研究.南京航空航天大学 302 信箱 210016.

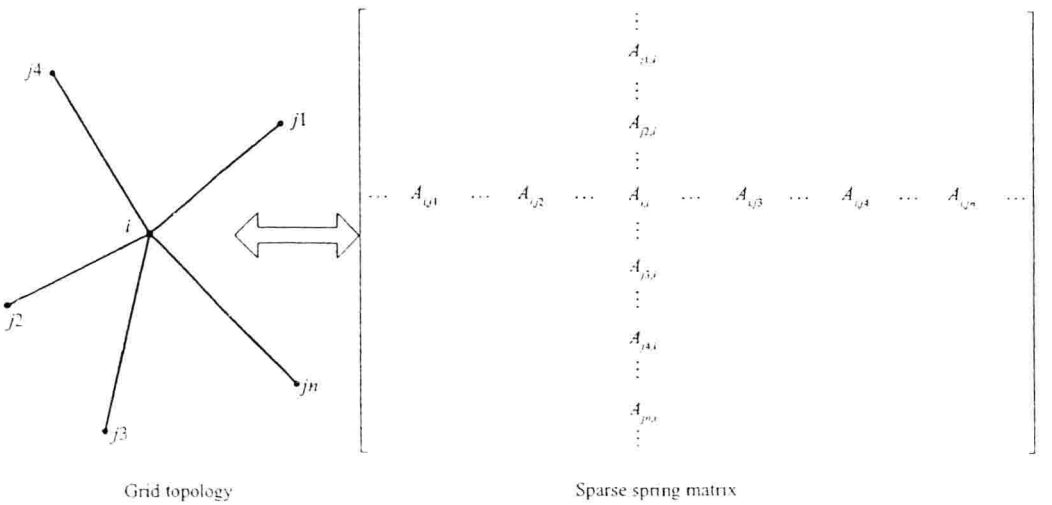

图 1　网格拓扑关系与弹簧模型系数阵的映射($j1 < j2 < i < j3 < j4 < \cdots < jn$)

Fig.1　Mapping of grid topology and sparse spring matrix($j1 < j2 < i < j3 < j4 < \cdots < jn$)

根据弹簧原理,i 点位移仅受周围网格点及自身位移量支配而与其它网格点无关,因此 $\boldsymbol{A}$ 矩阵非零元素排布与网格点拓扑关系可简述为 i 行的元素代表相邻点对 i 点的影响,i 列元素代表 i 点对相邻点的影响.设网格点 i 与 $j1, j2, j3, j4, \cdots, jn$ 等点相邻(图 1 中 n 为 5)且标号关系为 $j1 < j2 < i < j3 < j4 < \cdots < jn$,则 $\boldsymbol{A}$ 矩阵中所对应的第 i 行仅存在非零项 $A_{i,j1}, A_{i,j2}, A_{i,j3}, A_{i,j4}, \cdots, A_{i,jn}$,且依据网格点标号大小顺序分布于 $\boldsymbol{A}$ 矩阵的下三角阵、对角线与上三角阵中.同理,根据 i 点对相邻点的影响关系可得,第 i 列的非零项为 $A_{j1,i}$, $A_{j2,i}, A_{i,i}, A_{j3,i}, A_{j4,i}, \cdots, A_{jn,i}$,且依据网格点标号大小顺序分布于 $\boldsymbol{A}$ 矩阵的上三角阵、对角线与下三角阵中.由于任意两网格点之间的相互影响是等价的,即 $A_{ij} = A_{ji}$,显然 $\boldsymbol{A}$ 矩阵为对称矩阵,这与上述行列元素分布一致,且 $\boldsymbol{A}$ 矩阵为典型的大型稀疏矩阵,故需采用稀疏矩阵存储及记录方式处理,以保证计算资源的有效利用.

不同弹簧模型的拓扑关系是一致的,仅仅是弹簧刚度及位移系数矩阵各元素的计算方法有所区别.求解此方程可获得网格节点随边界的移动量.网格拓扑关系与稀疏系数矩阵的映射关系仅与网格点编号顺序有关,与弹簧模型的选取无关.

1.1　棱边(Segment)弹簧模型

棱边弹簧模型系假设每一网格边悬挂一个静平衡的弹簧,并具有标量刚度[3].i, j 点组成的棱边刚度定义为 K_{ij},则(1)式中位移矩阵 $\boldsymbol{A}$ 中第 i 行的系数写作

$$A_{ij} = \begin{cases} -K_{ij}, & i \neq j, \\ \sum\limits_{k} K_{ij}, & i = j, \end{cases} \tag{2}$$

显然,A 矩阵为对称矩阵,对角元为非零实数且占优.

1.2　线性(Linear)弹簧模型

三维线性弹簧模型采用平衡力构建网格节点的相互位移关系,θ 是所求的弹簧边在 xy 平面上的投影与 x 轴正向的夹角,φ 为弹簧边与 z 轴正向的夹角[3].对于 i 节点外的任意相连点 j,(1)式中位移矩阵 $\boldsymbol{A}$ 中第 i 行系数写作

$$A_{ij} = \begin{cases} K_{ij}\begin{bmatrix} -\cos^2\theta\sin^2\phi & -\cos\theta\sin\theta\sin^2\phi & -\cos\theta\sin\phi\cos\phi \\ -\cos\theta\sin\theta\sin^2\phi & -\sin^2\theta\sin^2\phi & -\sin\theta\sin\phi\cos\phi \\ -\cos\theta\sin\phi\cos\phi & -\sin\theta\sin\phi\cos\phi & -\cos^2\phi \end{bmatrix}, & i \neq j, \\ \sum\limits_{k} K_{ik}\begin{bmatrix} \cos^2\theta\sin^2\phi & \cos\theta\sin\theta\sin^2\phi & \cos\theta\sin\phi\cos\phi \\ \cos\theta\sin\theta\sin^2\phi & \sin^2\theta\sin^2\phi & \sin\theta\sin\phi\cos\phi \\ \cos\theta\sin\phi\cos\phi & \sin\theta\sin\phi\cos\phi & \cos^2\phi \end{bmatrix}, & i = j. \end{cases} \tag{3}$$

注意到,线性弹簧模型下,位移系数矩阵 A 为块矩阵(Block Matrix),A 阵中的元素为矩阵.分析(3)式可知 $A_{ij}(i\neq j)$的秩为 1,说明对于相连的两个网格点,一个点对另一点的位移影响仅发生在其连线所在的方向上,这与线性弹簧模型的假设相吻合.同时可知,A_{ii}为满秩矩阵,这保证了 i 节点可以向任意方向运动,并满足了线性方程组有唯一解的条件.

从本节对两种弹簧网格模型的分析可以看出,其位移系数矩阵的非零元分布不依赖于模型,但系数矩阵中的元素与弹簧模型密切相关.棱边弹簧中矩阵元素为实数,线性弹簧中矩阵元素为矩阵,且其均为非零项.这一特点是下节引入 LU-SGS 迭代算法的必要条件.

2 LU-SGS 网格迭代算法

构建基于弹簧原理的动网格算法,包括两个关键的数学处理步骤:①建立网格位移的线性方程组;②求解此线性方程组.其中①已在 1 节中详细叙述,本节论述求解算法.

对于上述几种常用弹簧网格模型,通常的算法均为 SOR 算法或 Gauss-Seidel 算法[2,3],受计算流体力学中隐式时间推进求解的 LU-SGS 算法启发,本文提出利用 LU-SGS 分解算法求解基于弹簧模型的常系数方程组,即求解 $Aq=B$,获得了理想的结果,以下给出算法的构建过程.

按拟时间步推进可得

$$\begin{cases} Aq^n = B^n \\ Aq^{n+1} = B^{n+1} \end{cases} \Rightarrow A(q^{n+1}-q^n) = (B^{n+1}-B^n) \Rightarrow A\Delta q^n = \Delta B^n . \tag{4}$$

由弹簧网格原理可知 $B=0$,当 $n\to\infty$,$\Delta B^n\to 0$,$\Delta q^n\to 0$,故 q 趋近于稳定解,且与 $Aq=B$ 相容.进一步将式(4)改写成

$$A\Delta q^n = 0 - B^n = -Aq^n, \quad \text{且 } q^n = q^{n-1} + \Delta q^{n-1}, \tag{5}$$

(5)式左侧 A 矩阵可写作

$$A = U + D + L, \tag{6}$$

U 为绝对上三角矩阵,L 为绝对下三角矩阵,D 为对角矩阵.(6)式写作

$$(D+L)D^{-1}(D+U)\Delta q^n = -B^n + (LD^{-1}U)\Delta q^n . \tag{7}$$

$\Delta q^n\to 0$,故进一步将(7)式写作

$$(D+L)D^{-1}(D+U)\Delta q^n = -Aq^n . \tag{8}$$

引入过渡变量 $\Delta q^{*n} = D^{-1}(D+U)\Delta q^n$,则

$$\begin{cases} (D+L)\Delta q^{*n} = -Aq^n , \\ (D+U)\Delta q^n = -D\Delta q^{*n} . \end{cases} \tag{9}$$

显然,(9)式通过一次下三角扫描由 q^n 求得 Δq^{*n},和一次上三角扫描由 Δq^{*n} 求得 Δq^n,进而获得 $q^{n+1}=q^n+\Delta q^n$,从而实现一个拟时间步推进.以 Δq^n 作为收敛判据,当 $\Delta q_1^n<\varepsilon$ 时,迭代停止,通常取 $\varepsilon=1.0\times10^{-5}$.需要特别说明的是,式(7)~(9)表明,若要 D^{-1}有意义,必须 A 矩阵主对角元非零(若对角元为方阵,则必须可逆),此即 LU-SGS 迭代算法的限制.经验表明,若 A 矩阵主对角占优,算法可靠性更佳.显然,弹簧模型中位移系数矩阵对角元非零且占优,特别适合此算法.

对运动网格而言,新时间层的网格点 p^{t+1}由上时间层的网格点坐标叠加网格点位移后获得,即 $p^{t+1}=p^t+q^t$.特别地,对于线性弹簧模型,A 矩阵元素为方阵,前向及后向扫描时,对角线上的元素需进行求逆操作.考虑到 A 矩阵为常系数阵,有必要单独存储对角元的逆矩阵,以提高计算效率.

3 边界网格运动管理策略

传统的用于非定常计算的动网格一般不涉及网格管理问题,因为其计算域一般总是由已知主动位移的运动边界和不运动的远场边界构成[2],其边界点运动总是唯一确定的.而本文所述的运动间断拟合问题则需面临更复杂的网格运动模式[4],为此本文采用了网格运动管理策略技术.策略包含两部分内容:①求解运动间断拟合过程中,边界位移处理技术;②边界点位移约束与弹簧模型相容性处理技术.

对具有运动间断的拟合问题，我们将所有的网格点划分为四类：

①运动边界点，由运动间断边界条件[4]确定位移量的边界网格点；

②固定边界点，位移量为 0 的固定点；

③牵连边界点，位移满足一定关系的边界点；

④内点，计算域内部的网格点．

以下节中将要给出的算例 1 为例，图 2 给出了该例的网格点分类．在这个超声速来流条件下的尖头体算例中，前缘点为指定的固定边界点，运动激波和柔性壁面为运动边界点，由运动边界条件决定其位移[4]，下游边界由于 A、B 两点的位置变化作牵连运动，但仍保持处于 AB 直线上，且网格点不发生交错，内点随弹簧模型运动．

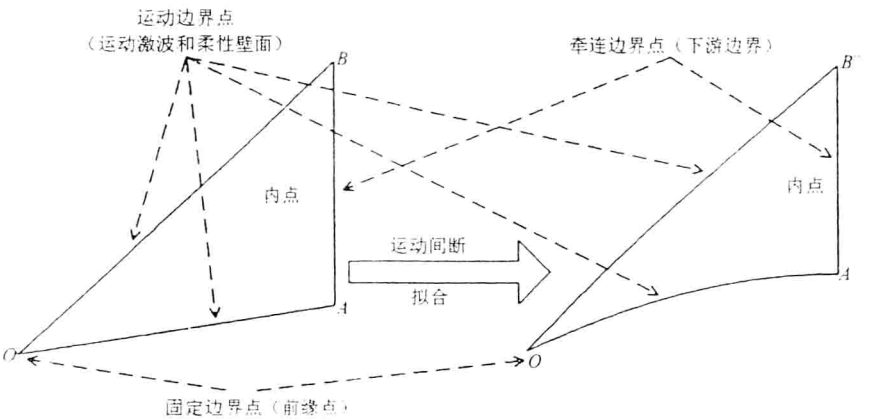

图 2　网格点运动类型示意

Fig. 2　Strategy of grid moving

对各网格点的位移量 q 的求解，在每一迭代步对不同类型网格点作不同处理，以保证与弹簧模型相容．运动边界点位移量由运动间断边界条件确定，故 $\Delta q = 0$，q 为已知量；固定边界点位移为 0，故 $\Delta q = 0$，$q = 0$；内点由弹簧模型确定位移，故 $\Delta q = \Delta q^*$，即迭代步获得的位移量新值；牵连边界点处理较为复杂．Δq^* 不仅由迭代获得，还应满足一定约束．本例中，AB 边内的点运动应服从于 AB 直线，故 Δq^* 应满足 AB 直线方程，即每一迭代步后，Δq^* 需经直线方程修正后，方可作为网格点的 Δq．

4　数值算例

本文算例系由作者及所在课题组独立开发的面向流体的通用仿真系统 Focuss-CFD（Fluid Oriented Combined Universal Simulation System-Computational Fluid Dynamic）完成，编程语言为 C++，运行环境为 PC-P4-3.0G．

4.1　二维尖头体

超声速来流条件下，二维尖头体上的流场可由特征线法获得解析解[5]．按文[5]构建算例，二维型面及表面压力分布如图 3(a)所示．图 3(b)给出了本文算法的初场设置，$Ma_\infty = 3.0$，计算域长度为 3.291，前缘点位置(0.0,0.0)，A、B 点 x 坐标为 3.291，其 y 坐标及 $\angle AOB$ 任意指定，无特殊要求．在 OA 边界上采用运动激波边界条件；OB 边界采用运动壁面（柔性壁）边界条件[4]，并按图 3(a)所示，指定柔性壁上的压力分布，$p/p_\infty \in [1.0,7.0]$；AB 边界为压力远场边界条件．图 3(c)给出了一个典型结果，对于本文所采用的各种算法组合，其计算结果均一致．流场计算收敛后获得稳定曲线激波和尖头体型面，反求所得型面与预期型面一致；激波形状准确清晰，其精度明显高于捕获法，与特征线法相当．

表 1,2 给出了此算例条件下，不同弹簧模型及不同解算方法下的计算耗时情况．考虑到流场计算初期计算域及网格变形较大，动网格耗时较多，而计算后期计算基本稳定，动网格迭代步大幅减小，因此，仅取计算开始后 500 个流场时间推进步内的时耗作为对比依据．

对比 Case1 ~ Case8 可以看到，在网格运动最为剧烈的计算时期内，不论是隐式时间推进还是显式时间推

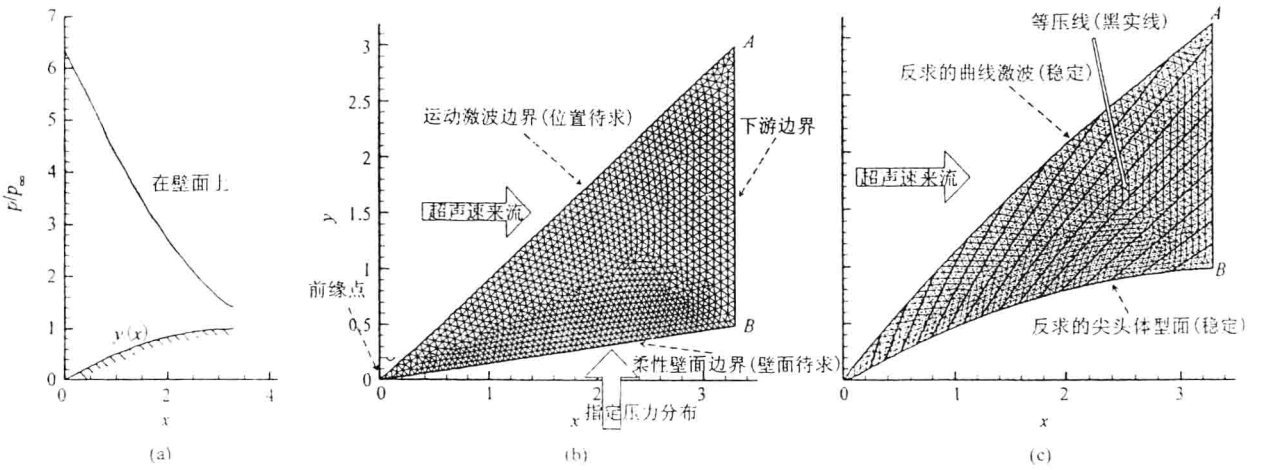

图 3 尖头体算例

Fig.3 Wedge computation

进，采用 LU-SGS 网格迭代算法较 SOR 方法均有 23% ~ 42% 的时耗降低. 同时，对于不同的弹簧模型，LU-SGS 网格迭代算法均可适用，不同的弹簧模型及解算方法对最终获得稳定解没有影响. 因此，从 LU-SGS 迭代算法与各弹簧模型和显隐时间格式的兼容性表现来看，使其完全可以作为一个独立算法模块，与其他数值计算方法组合使用，以发挥更为优良的性能.

在研究过程中还发现，结构化网格条件下，LU-SGS 算法的耗时与 SOR 算法接近. 其原因当归结为结构化网格自身拓扑关系的特点，结构化网格的稀疏系数阵接近于一个带状矩阵，在此情况下，SOR 方法的迭代效率将会大幅改善，使其与 LU-SGS 迭代算法的效率相当.

表 1 算例耗时对比

(显示时间推进，流场时间推进步 500)

Table 1 Computation time in different cases

(exp, 500steps)

Case	弹簧模型	网格算法 (松弛因子)	CFL	整体耗时/s
1	Segment	SOR (1.3)	0.5	340
2	Segment	LU-SGS(-)	0.5	275
3	Linear	SOR (1.3)	0.5	671
4	Linear	LU-SGS (-)	0.5	569

表 2 算例耗时对比

(隐式时间推进，流场时间推进步 500)

Table 2 Computation time in different cases

(imp, 500steps)

Case	弹簧模型	网格算法 (松弛因子)	CFL	整体耗时/s
5	Segment	SOR (1.3)	1.0	366
6	Segment	LU-SGS(-)	1.0	257
7	Linear	SOR (1.3)	1.0	692
8	Linear	LU-SGS (-)	1.0	539

4.2 三维三角形乘波翼

超声速流场中，乘波机翼在一定前缘攻角下于下表面上产生一道激波，激波形状随前缘形状及攻角不同而变化，且于下表面上产生高压，以此获得升力[7]. 三角翼即属于此类乘波翼形，在非设计状态下其激波面为三维曲面. 针对给定的三角翼，应用本文算法可求解任一马赫数下的曲面激波形状.

图 4(a)为初始三角乘波翼形状，其中三角翼顶角 θ 为 126.0°，攻角 α 为 11.3°，来流马赫数 3.0. 图 4(b)，图 4(c)分别从前侧方和后侧方展示了初始计算域及网格形状，乘波翼 OAB 仍采用一般的固壁边界，仅在激波面 OAC 和 OBC 采用运动激波边界条件[4]，以求解激波形状，平面 ABC 为出流边界. 运动计算域下求解流场时，须同时将流场残值与网格点位移量作为收敛参考依据. 流场相对残值应小于 $\varepsilon = 1.0 \times 10^{-6}$，网格点位移量相对与网格尺寸也应小于 $\varepsilon = 1.0 \times 10^{-6}$.

采用不同的流场时间推进算法、弹簧网格模型和动网格迭代算法，求解翼形上的曲面激波形状. 图 5 给出了一个典型的计算域变化历程和最终结果，其视图角度与图 4(b)一致. 三维流动条件下，仍可以获得准确光滑的曲面激波形状. 各计算条件下的耗时对比见表 3、表 4，同等条件下，采用 LU-SGS 迭代算法比 SOR 方法节约了 12% ~ 22% 的计算时耗，尤其是隐式时间推进下采用棱边弹簧模型 LU-SGS 迭代算法获得的计算效率最佳.

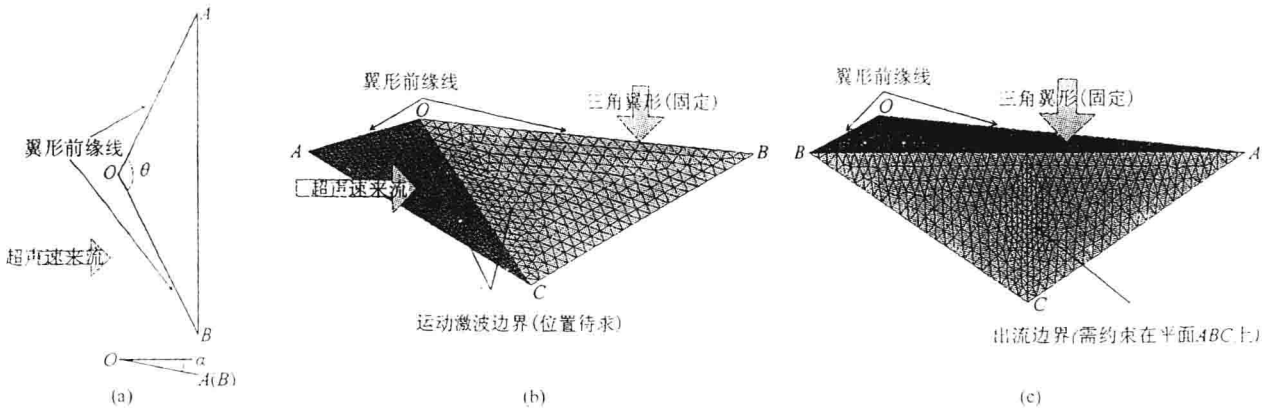

图 4　三角形乘波翼初始计算域及网格

Fig.4　Initial grid of tri-wing computation

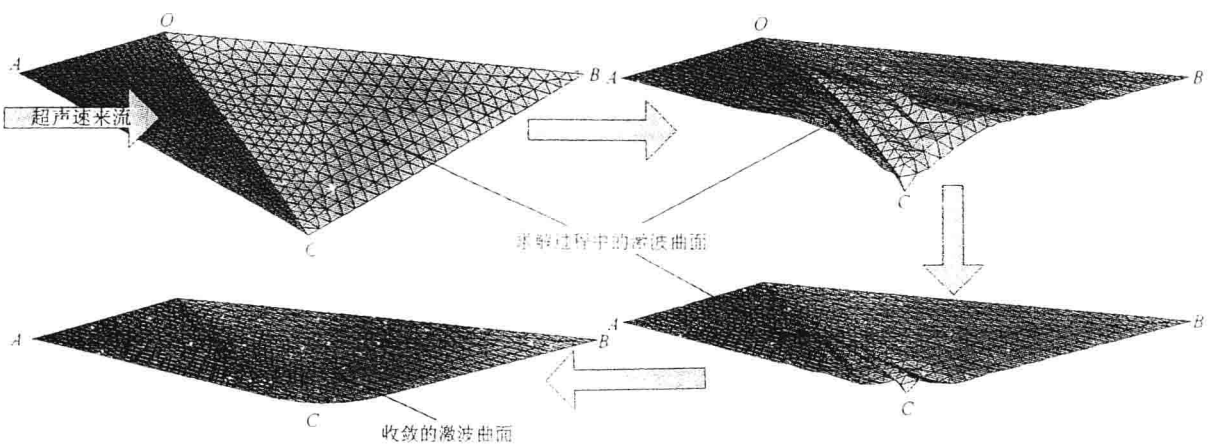

图 5　求解过程中的计算域及网格变化

Fig.5　Process of grid moving in tri-wing computation

表 3　算例耗时对比

(显示时间推进,流场时间推进步 500)

Table 3　Computation time in different cases

(exp, 300steps)

Case	弹簧模型	网格算法(松弛因子)	CFL	整体耗时/s
1	Segment	SOR (1.3)	0.5	275
2	Segment	LU-SGS(=1)	0.5	245
3	Linear	SOR (1.3)	0.5	578
4	Linear	LU-SGS(=1)	0.5	511

表 4　算例耗时对比

(隐式时间推进,流场时间推进步 200)

Table 4　Computation time in different cases

(imp, 200steps)

Case	弹簧模型	网格算法(松弛因子)	CFL	整体耗时/s
5	Segment	SOR (1.3)	0.5	282
6	Segment	LU-SGS(=1)	0.5	231
7	Linear	SOR (1.3)	0.5	565
8	Linear	LU-SGS(=1)	0.5	503

5　结论

本文针对运动间断拟合算法中计算域及网格需在每一时间推进步后更新的特点,提出了一种新的快速网格迭代算法——LU-SGS 网格迭代算法,并采用棱边弹簧模型和线性弹簧模型分别在二维和三维算例上进行了对比验证,得出以下结论:

1)基于弹簧网格原理给出了网格拓扑关系与稀疏系数矩阵的映射关系,提出了依赖于网格点编号和网格拓扑关系的位移稀疏系数矩阵构建原理与方法,将弹簧网格的迭代归结为一个大型稀疏常系数线性方程组的求解问题,理论上适用于任何形式的弹簧模型;

2)弹簧网格模型下的位移系数矩阵满足 LU-SGS 迭代算法的使用条件限制,算法适用于二维和三维条件下运动间断拟合的求解.在非结构网格流场隐式时间推进下,辅以恰当的网格运动策略,能保持获得稳定解,且计算快速、准确,激波分辨率高;

3)LU-SGS 网格迭代算法在非结构网格条件下,可大大缩短网格迭代耗时.就本文算例而言,计算整体时耗较 SOR 算法降低了 12% ~ 42%;

4)不同的弹簧模型、网格迭代算法及流场时间步推进算法对最终获得运动间断拟合的稳定解没有影响.在一般的运动间断拟合问题的求解中,可选择较为简单的弹簧网格模型,并采用 LU-SGS 迭代算法,尽可能缩短动网格耗时,提高计算效率.

[参 考 文 献]

[1] Wang Ruili, Yao Yanzhong, Lin Zhong, Ge Quanwen. A new unstructured quadrilateral mesh generation application[J]. Chinese J Comput Phys, 2007, **24**(1): 13 - 18.

[2] Zhang Yudong, Ji Chuqun. Numerical methods with dynamic structured meshs for unsteady flows with moving boundaries[J]. Chinese J Comput Phys, 2006, **23**(2): 165 - 170.

[3] Clarence O E Burg. A robust unstructured grid movement strategy using three-dimensional torsional springs [R]. 34th AIAA Fluid Dynamics Conference and Exhibit. AIAA 2004 - 2529, 2004.

[4] 吴晴,钟易成,余少志.一种基于运动间断拟合的型面反设计数值方法[C]//第十三届全国计算流体力学会议,辽宁丹东,2007.

[5] 左克罗 M J,霍夫曼 J D.气体动力学[M].国防工业出版社,1984:173 - 185.

[6] 屈奇曼 D.飞机空气动力设计[M].航空工业部第 603 研究所,1983:343 - 350.

An Iterative Method For Unstructured Dynamic-grid Using Springs Based on LU-SGS

WU Qing, ZHONG Yicheng, YU Shaozhi, HU Jun

(*College of Energy and Power Engineering, Nanjing University of Aeronautics and Astronautics, Nanjing* 210016, *China*)

Abstract: An iterative method for unstructured dynamic-grid using springs based on LU-SGS (lower-upper symmetric Gauss-Seidel) is presented to reduce time of iterative in dynamic discontinuities simulation. Dynamic grid iterative time is as much as time of field iterative as shock and flex-wall are numerical fitting by time-dependent Euler equations, because dynamic boundary is moving and whole unstructured grids are updated in every step of field iterative. A sparse matrix mapping grid topology based on spring strategy is presented. LU-SGS strategy is used in numerical simulation and dynamic grid is managed in order to solve the time choke point. Numerical results show that LU-SGS iterative method can be used to dynamic discontinuities fitting by implicit scheme. The presented method decreases more than 20% iterative time than classical SOR method.

Key words: dynamic grid; LU-SGS; spring model; dynamic discontinuities fitting; computational fluid dynamic(CFD)

Received date: 2008 - 06 - 17; **Revised date**: 2008 - 12 - 06

Navier-Stocks Computations of Wind-Turbine Airfoil using Low Mach Number Preconditioning

Wu Qing, Zhong Yicheng, Hu Jun, Yu Shaozhi
College of Energy & Power Engineering,
Nanjing University of Aeronautics and Astronautics
CEPE NUAA
Nanjing, China
nuaawuqing@nuaa.edu.cn

***Abstract*—Wind turbine airfoil is numerical simulated by using the governing equations of compressible fluids in this paper. The Reynolds Averaged Navier-Stocks computations are combined with low Mach preconditioning and implicit matrix-free Lower-Upper Symmetric Gauss-Seidel(LUSGS) iteration on unstructured meshes, and the results are improved at the very low velocity speeds which are representative of the flow field around a wind turbine airfoil. Detailed LUSGS algorithm with preconditioning is present in this paper, which is improved to cost less data storage and computational time for steady flow. The steady and unsteady characteristics of static 2D-S809 airfoil are analyzed by the numerical results and compared between calculations and tests. Aerodynamic coefficients have been got using the algorithm of this work at all angles of attack. The unsteadiness induced separation bubble shedding has been captured by this method finally.**

Keywords: wind turbine airfoil; preconditioning; unsteady flow; LUSGS

I. INTRODUCTION

Wind energy is regenerative energy with the characteristics of clean, low cost and affluent in storage. Wind turbine airfoil is an important part of the whole wind generator, but little work is done on this research field, and the technology is poor in china.

Aerodynamic performance computation is an essential step in the design of wind turbine. The calculation results can be used to modify the profile of the 2-D airfoil and design the twisted 3-D blade, and 2-D airfoil's aerodynamic characteristics are the basic design condition for these works. Experiments and numerical simulations have being done in these years [1-5], but there are many differences between them. Compared with the tests, numerical simulations are more rapid and cheap, but not very exactly.

At low Mach number around the wind turbine, CFD simulation for compressible flow is invalid without preconditioning, and the convergence is very slowly. A detailed dual time-stepping algorithm with Preconditioning [6] and implicit LUSGS iteration [7] is accordingly presented and improved in this paper. Some steady and unsteady numerical results for static airfoil are analyzed and compared with the tests.

The program of this numerical algorithm is developed by authors and introduced into our CFD software system which is named FOCUSS-CFD (Fluid Oriented Combined Universal Simulation System - Computational Fluid Dynamic).

This work was supported by National Basic Research Program of China (973 Program) (No. 2007CB210301).

II. METHODS

A. Dual time-stepping algorithm with Preconditioning

1) Governing Equations

For the general problem of compressible flows in a fixed computational domain Ω, the time-duel compressible Navier–Stokes equations can be written as:

$$\frac{\partial}{\partial t}\int_{\Omega} U dV + \oint_{\partial\Omega} F(U) - F_v(U) dS = 0 \qquad (1)$$

where U represents the vector of conserved variable (mass, momentum and energy), and $U = [\rho, \rho u, \rho v, \rho w, \rho e]^T$. $F(U)$ represents the convective fluxes and $F_v(U)$ represents the viscous fluxes, $\partial\Omega$ is the boundary of domain Ω, and dS is area of interface $\partial\Omega$ respectively.

For retaining the time accuracy, A dual time-stepping procedure is employed to solve the unsteady flow. A preconditioned pseudotime-derivative term is introduced into (1) as following:

$$\Gamma\frac{\partial}{\partial \tau}\int_{\Omega} Q dV + \frac{\partial}{\partial t}\int_{\Omega} U dV + \oint_{\partial\Omega} F(U) - F_v(U) dS = 0 \qquad (2)$$

where τ and t denote pseudotime and physical time respectively, Γ is a preconditioning matrix and $Q = [p, u, v, w, T]^T$ are primitive variables. Note that as $\tau \to \infty$, the first term on the left-hand side of (2) vanishes and (1) is recovered. This approach involves an inner iteration loop in pseudotime that is wrapped by an outer loop stepping through physical time. The solution at each physical time level is treated as a steady state problem in pseudotime.

the preconditioning matrix Γ is defined by:

$$\Gamma = \begin{bmatrix} \theta & & & & \rho_T \\ \theta u & \rho & & & \rho_T u \\ \theta v & & \rho & & \rho_T v \\ \theta w & & & \rho & \rho_T w \\ \theta H - 1 & \rho u & \rho v & \rho w & \rho_T H + \rho Cp \end{bmatrix}$$

Where for ideal gas, θ is defined as,

$$\theta = \rho_p' = (\frac{1}{V_r^2} - \frac{\rho_T}{\rho Cp}) = \frac{1}{c^2 M_r^2} + \frac{1}{TCp} = \frac{1+(\gamma-1)M_r^2}{TM_r^2} = \frac{1}{\alpha T}$$

$$\text{where } \alpha = \frac{M_r^2}{1+(\gamma-1)M_r^2}$$

$\beta = M_r^2$ is the preconditioning parameter, which is defined as:

$$\beta = \min(\max(M_{local}^2, M_{r\min}^2), 1.0)$$

the local Mach Number is the maximum value around the ctrl volume(including neighbour ctrl volumes), and $M_{r\min}^2 \approx 3M_\infty^2$. For the external flow, the M_∞ is incoming free stream Mach number.

The eigenvalues of the system matrix are:

$$\tilde{\Lambda} = \begin{bmatrix} q_n & & & & \\ & q_n & & & \\ & & q_n & & \\ & & & \frac{(\beta+1)q_n + S}{2} & \\ & & & & \frac{(\beta+1)q_n - S}{2} \end{bmatrix} \quad (3)$$

Where q_n is the flow velocity normal to the surface of the control volume, and $S = \sqrt{q_n^2(\beta-1)^2 + 4\beta c^2}$.

Note that as $M_\infty \to 1$, $\beta \to 1$, the preconditioned equations reduce to the original governing equations. For low speed flows, β is small and the wave speeds are modified so that all the eigenvalues possess the same order of magnitude. The system stiffness problem has been overcome.

The eigenvariables of the modified system matrix are:

$$\partial W = \begin{bmatrix} k_x[\frac{-(\gamma-1)}{\rho}\partial p + \partial T] + (k_z\partial v - k_y\partial w) \\ k_y[\frac{-(\gamma-1)}{\rho}\partial p + \partial T] + (k_x\partial w - k_z\partial u) \\ k_z[\frac{-(\gamma-1)}{\rho}\partial p + \partial T] + (k_y\partial u - k_x\partial v) \\ \partial p + \rho(\lambda_4 - \beta q_n)\partial q_n \\ \partial p + \rho(\lambda_5 - \beta q_n)\partial q_n \end{bmatrix} \quad (4)$$

The equations of the system are nondimensionalized by free stream density, speed of sound, temperature, viscosity conductivity, and a reference length. As the results, the sound speed and the states equation are:

$$c^2 = T, \quad \rho = \frac{\gamma p}{T}$$

2) Spatial discretization scheme

For the fixed grid, Equation (2) can be discretized in a polygonal control volume V_i as:

$$\Gamma_i V_i \frac{\partial Q}{\partial \tau} + V_i \frac{\partial U}{\partial t} + RES_i(U) = 0 \quad (5)$$

RES_i is the residual given by:

$$RES_i = \sum_{j=1}^{nface} (F(U) - F_v(U))S_{ij} \quad (6)$$

Because of the preconditioning matrix Γ, the inviscid flux is calculated using a reformulated Roe-type flux difference splitting scheme,

$$\tilde{F}_{ij} = \frac{1}{2}(F(Q_i, n_{ij}) + F(Q_j, n_{ij}) - \Gamma X|\tilde{\Lambda}|\partial W) \quad (7)$$

where $\tilde{\Lambda}$ is the modified eigenvalues , X is the matrix of right eigenvectors, respectively.

The primitive variables reconstructed by a weighted least square linear reconstruction scheme at both sides of a ctrl face are used in (7). The second order interpolation is applied to the reconstruction procedure not only to supply the better accuracy, but also to prevent oscillations in non-smooth regions.

3) Temporal discretization

The pseudotime term in (4) is discretized with a first order backward difference and the physical time term is discretized in an implicit fashion by a second order backward difference.

$$(\frac{1}{\Delta\tau}\Gamma_i + \frac{3}{2\Delta t}M_i)V_i\Delta Q_i + RES_i^*(Q^{m+1}) = 0 \quad (8)$$

$$RES_i^*(Q^{m+1}) = V_i(\frac{3U^m}{2\Delta t} - \frac{2U^{n-1}}{\Delta t} + \frac{U^{n-2}}{2\Delta t}) + RES_i(Q^{m+1}) \quad (9)$$

Where $\Delta Q_i = Q^{m+1} - Q^m$, $U^{n+1} = U^{m+1} + M\Delta Q$, and $M = \frac{\partial U}{\partial Q}$, also m and n denote pseudotime and physical time inter respectively. Note that if the Q^{m+1} is instead to Q^m, equation(8) and (9) vanish to explicit time-stepping fashion in pseudotime term. Obviously, once the terms about the physical time are called off, these equations recover the solution of steady flow.

B. *Implicit Matrix-Free LUSGS*

Hong Luo's Implicit Matrix-Free LUSGS [7] is a better choice of this solution, and the algorithm with preconditioning is considered in this paper.

The residual term $RES_i(Q)$ at the $m+1$ pseudotime level is linearized giving the following equations:

$$[(\frac{\Gamma_i}{\Delta\tau} + \frac{3M_i}{2\Delta t})V_i + \frac{\partial RES(Q)}{\partial Q_i})]\Delta Q_i + \frac{\partial RES(Q)}{\partial Q_j}\Delta Q_j = -RES_i^*(Q^m) \quad (10)$$

To simplify the implicit time-step calculation, the first order numerical flux vectors in the left-hand side of the above equation is chosen as

$$RES(Q) = \frac{1}{2}(\tilde{F}_i + \tilde{F}_{ij} - \Gamma_{ij}\tilde{\lambda}_{ij}(Q_j - Q_i)) \quad (11)$$

As Luo Hong done, equation (10) is simplified as following with second physical time accuracy:

$$[(\frac{V_i}{\Delta\tau} + \frac{1}{2}\sum_{j=1}^{n}\tilde{\lambda}_{ij}S_{ij})I + \frac{3V_i}{2\Delta t}M_i\Gamma_i^{-1})]\Gamma_i\Delta Q_i = -RES_i^*(Q^m) - \frac{1}{2}\sum_{j=1}^{n}(\Delta\tilde{F}_j - \Gamma_j\tilde{\lambda}_{ij}\Delta Q_j)S_{ij} \quad (12)$$

We define $a = \frac{V_i}{\Delta\tau} + \frac{1}{2}\sum_{j=1}^{n} \widetilde{\lambda}_{ij} S_{ij}$, $b = \frac{3V_i}{2\Delta t}$, and

$D = aI + b \cdot Diag(M\Gamma^{-1})$. Equation (10) can be solved by using a Lower–Upper Symmetry Gauss-Seidel (LUSGS) scheme on unstructured grids.

Forwardsweep:

$$\Delta\widetilde{U}_i^* = D^{-1}[-RES_i^*(Q^m) - \frac{1}{2}\sum_{j:j\in Lower(i)}(\Delta\widetilde{F}_j - \widetilde{\lambda}_{ij}\Delta\widetilde{U}_j^*)S_{ij}] \quad (13)$$

Backwardsweep:

$$\Delta\widetilde{U}_i = \Delta\widetilde{U}_i^* - D^{-1}[\frac{1}{2}\sum_{j:j\in Upper(i)}(\Delta\widetilde{F}_j - \widetilde{\lambda}_{ij}\Delta\widetilde{U}_j^*)S_{ij}] \quad (14)$$

Where $\Delta\widetilde{U}_i = \Gamma\Delta Q_i$. Obviously, Matrix Γ^{-1} and M are required by this method for unsteady flow. Fortunately, when the steady flow is simulating, Matrix D vanishes to a real number, and just Γ^{-1} needs to be calculated and stored.

C. model and Grid

The S809 airfoil is designed for wind-turbine specifically in 1989[2], which of thickness is 21% chord. Lots of test reports are published in these years [1-3]. A sketch of the airfoil is shown in Figure 1. This airfoil also was chose to be the wind turbine model for our study. The numerical results are compared with these tests, and aerodynamic characteristics are analyzed at low speed in this paper.

The computational mesh is a block mesh with unstructured data storage, and contains boundary layer mesh block and external mesh block, see Figure 1. The mesh was generated by Gambit 2.3, and the geometry topology information was imported to our own CFD software by MSH file. The total of 53000 cells is all quadrilateral elements, and there are 408 cells around the body, see Figure 1. The cell thickness at the airfoil surface is $dh = 0.0001 * L_{chord}$, and there are 32 cells along the stream vertical direction with 1.2 ratio. Turbulence flow is assumed using the Spalart-Allmaras model without transition term. All calculations were made with Reynolds numbers of 2,000,000 or 500,000 at low Mach number for compressible flow.

III. Results and Discussion

A. Steady Aerodynamic Characteristics

Figure 2 through 4 show surface pressure distributions comparisons between the calculations and experiments at the Reynolds number 2,000,000. The airfoil chord is 0.6 m, and the free stream Mach number is 0.13333. Table 1 to 3 shows aerodynamic coefficients errors between the numerical simulated and the tested respectively.

For three angles of attack of 0°, 1.02° and 5.13°, the Cp comparisons show reasonably agreement over the entire airfoil surface except in the regions of the laminar separation bubbles. The results of some commercial CFD software are similar to this work [1], see Table 1. One reason of this error is the lack of detailed information on the inlet boundary conditions used in the experiment [2]. As Ochs [2] said, the actual laminar flow is not to be simulated on the leading edge region. In fact, for numerical simulations, such laminar separation bubbles are very difficult to be captured with the RANS. The differences between the measured values and the calculated are 12%-20% on lift coefficients, see Table 1 through 3.

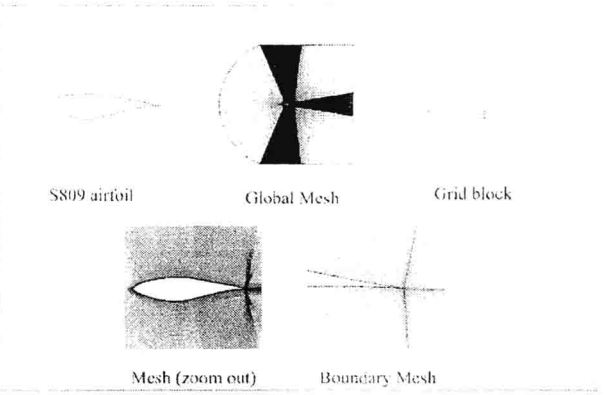

Figure 1. S809 airfoil and computational field mesh

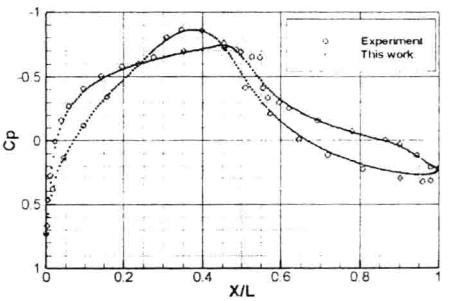

Figure 2. Pressure Distribution for $\alpha = 0^\circ$

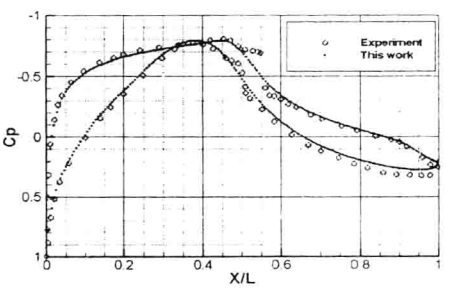

Figure 3. Pressure Distribution for $\alpha = 1.02^\circ$

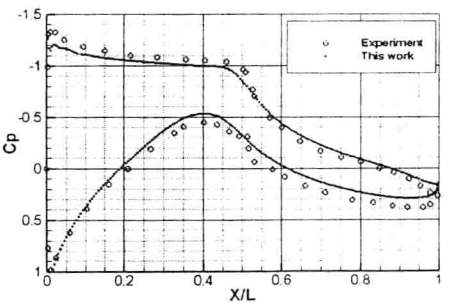

Figure 4. Pressure Distribution for $\alpha = 5.13^\circ$

TABLE.1 COMPARISON OF FORCES ($\alpha = 0^{\circ}$)

Parameter	*Cl*	*Diff, %*	*Cd*	*Diff, %*
Ochs's Exp	0.1469		0.0070	
Fluent	0.1178	19.8	0.0096	37.1
This work	0.1182	19.5	0.0041	41.4

TABLE.2 COMPARISON OF FORCES ($\alpha = 1.02^{\circ}$)

Parameter	*Cl*	*Diff, %*	*Cd*	*Diff, %*
Ochs's Exp	0.2716		0.0072	
This work	0.2295	15.5	0.0045	37.5

TABLE.3 COMPARISON OF FORCES ($\alpha = 5.13^{\circ}$)

Parameter	*Cl*	*Diff, %*	*Cd*	*Diff, %*
Ochs's Exp	0.7609		0.0070	
This work	0.6626	12.9	0.0093	32.9

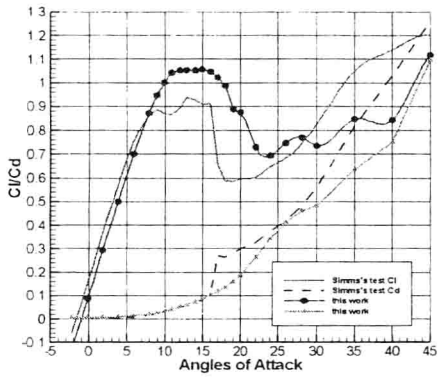

Figure 5. Comparisons of Lift and Drag coefficients

The calculations at higher angles of attack were analyzed with another experimental condition in this paper. The test results were reported by Simms and Hand in 1999 [3]. The Reynolds number is 500,000, the chord is about 0.45m, and the free stream Mach number is about 0.05. It is impossible to simulate the compressible flow at such Mach number without preconditioning, and the results are not good agreed with the actual flow. Hence, the algorithm with preconditioning for compressible flow is considered to solve this problem.

Figure 5 shows the comparisons between the calculated and experimental aerodynamic coefficients at all angles of attack with Simms's conditions. At the lower angles of attack, the lift coefficients are consistent with tests relative. The lift coefficients decrease from 0.95 to 0.6 between the angles of 10.0° and 30.0°, but the numerical results is higher than them. Over the airfoil upper surface, the trailing edge laminar separation point is moving forward with the angle of attack, and the separated bubble is changing larger. Because of the massively bubble, the pressure distribution around the airfoil includes a constant pressure region from the middle to trail section, see figure 6. For lack of accuracy for laminar flow modeling on the leading edge, the aerodynamic coefficients are not agree with tests between the angles of 10.0° and 30.0°. For the details of such flow including laminar and transition, CFD simulation is still weak. The results of other's current research are similar to our work [6].

For the static airfoil, the separation bubbles are still shedding frequently [5], which are similar to flow over a cylinder. At the high angle of attack, numerical simulation can not converge fluently for this unsteadiness by steady algorithm. The unsteady aerodynamic characteristic of static airfoil is considered in the next section by unsteady algorithm.

B. *Unsteady Aerodynamic Characteristics of static airfoil*

For angle of attack 18.0°, unsteady vortex shedding around the airfoil is calculated by the Dual time-stepping algorithm with preconditioning.

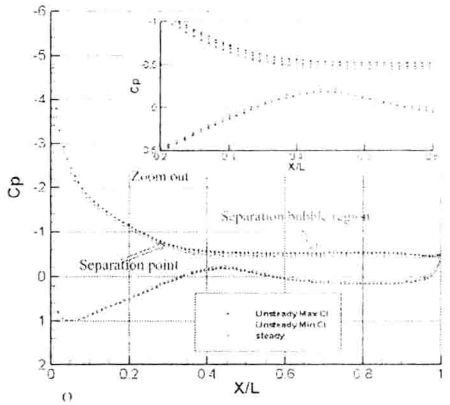

Figure 6. Unsteady Pressure Distribution for $\alpha = 18.0^{\circ}$

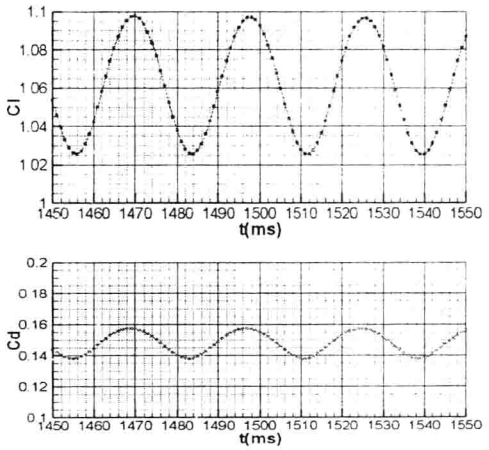

Figure 8. Comparisons Between steady and unsteady aerodynamic coefficients ($\alpha = 18.0^{\circ}$)

The physical time-step for this case was chosen to be 1.0 ms, 100 inner iterations were performed at each physical time level. The predicted cycle time can be found as about 0.028s.

Computed contours of stream vorticity around the airfoil are shown in Figure 7. It is shown in these pictures that the massively bubble of trailing edge separation is shedding periodically over the suction of the S809. The separation point is very far from trailing edge and is holding the fixed position. But the size of separation bubble is changing frequently and shedding with the constant frequency. Figure 6 shows the tiny differences of surface pressure distributions between steady and unsteady, which is tiny.

Because of these unsteady separation bubbles, the aerodynamic coefficients are wavy. Figure 8 shows the lift coefficients and the drag coefficients in the period including 3-4 cycle time. Due to turbulence and laminar flow both exist at such high Reynolds number around the 2D-airfoil, the turbulence simulation results are not agree with the tests so good. Another reason of this phenomenon is that the detailed conditions of the experiment are lack. However, the unsteadiness induced bubbles of static airfoil can be captured and the cycle time has been predicted by the algorithm of this work successfully.

IV. CONCLUSION

A dual time-stepping algorithm combined with low Mach preconditioning and implicit matrix-free Lower-Upper Symmetric Gauss-Seidel (LUSGS) iteration is considered in this paper detailed. The LUSGS iteration is improved to cost less data storage for steady calculation. The steady and unsteady stream around static wind-airfoil can be simulated by this method at low Mach number for compressible flow.

S809 was chose to be validated this numerical method, and the steady and unsteady aerodynamic characteristics were analyzed. Steady Computations at all angles of attack were completed in this paper, which were agreed with tests segmental. Unsteady flow has been computed for static airfoil by the dual time-stepping algorithm at 18.0° of attack angle with Reynolds number of 500,000 in 1.5 seconds. The predicted cycle time of unsteady flow is about 0.028s.

The 2-D and 3-D calculations of wind-turbine airfoil are basic complicated work for the design of the wind-turbine. In this paper, the aerodynamic coefficients have been got and the errors between experiments and calculation are present. Future work will focus on the 3-D simulations using unsteady RANS equations based-on the algorithm of this work.

REFERENCES

[1] *Valerio Viti, Development of an aerodynamic and aeroelastic tool for wind turbine design [J], 48th AIAA Structural, Structural Dynamics, and Materials Conference [C], AIAA-2007-2241, April 2007.*

[2] *Walter P. Wolfe, Stuart S. Ochs, CFD calculations of S809 aerodynamic characteristics [J], AIAA-97-0973, 1997.*

[3] *D. A. Simms, M. M. Hand, L. J. Fingersh, D. W. Jager, Unsteady aerodynamics experiment phases II-IV test configurations and available data campaigns [R], National Renewable Energy Laboratory, July 1999.*

[4] *Philip E.O. Buelow, Douglas A. Schwer, Jinzhang Feng, Charles L. Merkle, A preconditioned dual-time, diagonalized ADI scheme for unsteady computations[J], AIAA 97-2101, pp. 120–130, 1997.*

[5] *E.A. Mayda, C.P. van Dam, P.N. Duque, Bubble induced unsteadiness on wind turbine airfoils [J], AIAA-2002-0033, 2002.*

[6] *R.B. Langtry, J. Gola, F.R. Menter, Predicting 2D airfoil and 3D winf turbine rotor performance using a transition model for general CFD codes[J], 44th Aerospace Sciences Meeting and Exhibit[C], AIAA-2006-0395, 2006.*

[7] *Hong Luo, Joseph D. Baum, Rainald Lohner, A fast, matrix-free implicit method for compressible flows on unstructured grids [J], Journal of Computational Physics, vol. 146, pp. 664-690, 1998.*

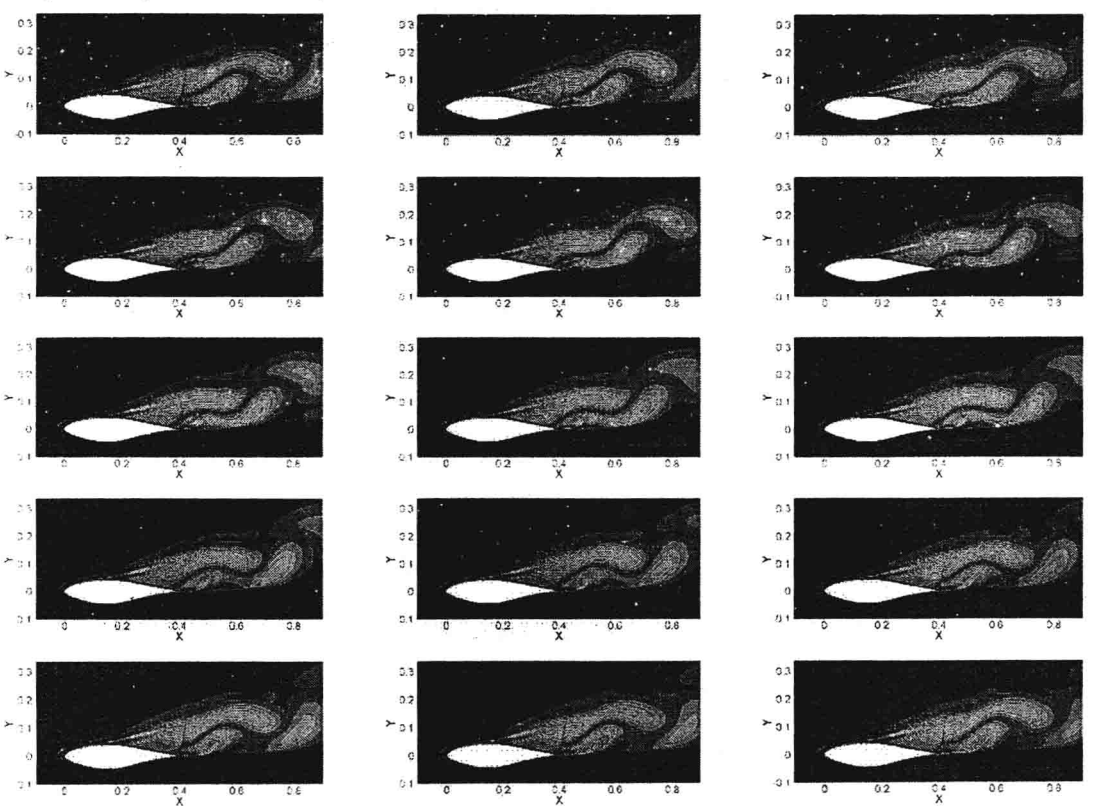

Figure 7. Process for the contour of unsteady stream vorticity around the airfoil at $\alpha = 18.0^{\circ}$ ($t_{cycle} \approx 0.028s, t_{\text{described}} = 0.03s$)